Bed load at low shields stress on arbitrarily sloping beds: Failure of the Bagnold hypothesis

(Article begins on next page)

13 May 2024

Bed load at low Shields stress on arbitrarily sloping beds: Failure of the Bagnold hypothesis

Giovanni Seminara and Luca Solari[1]

Dipartimento di Ingegneria Ambientale, Università degli Studi di Genova, Genova, Italy

Gary Parker

St. Anthony Falls Laboratory, University of Minnesota, Minneapolis, Minnesota, USA

[1] The Bagnold hypothesis has been a major tool in the development of mechanistic models of bed load transport. According to the hypothesis, a necessary constraint for the maintenance of equilibrium bed load transport is that the fluid shear stress at the bed must be reduced to the critical, or threshold value associated with incipient motion of grains. The constraint determines a functional form for the areal concentration of bed load grains as a function of flow parameters. It is shown here, however, that the Bagnold hypothesis breaks down when applied to equilibrium bed load transport on beds with transverse slopes above a relatively modest value that is well below the angle of repose. In particular, under such conditions it is shown that no areal concentration, no matter how large, is sufficient to reduce the fluid shear stress at the bed to the critical value. This failure motivates the abandonment of the Bagnold constraint, even for nearly horizontal beds. The framework presented here, however, provides a natural basis for an entrainment-based model of sediment transport that neither satisfies nor suffers from the drawbacks of the Bagnold constraint.   *INDEX TERMS:* 1815 Hydrology: Erosion and sedimentation; 1824 Hydrology: Geomorphology (1625); 3210 Mathematical Geophysics: Modeling; *KEYWORDS:* bedload, Shields stress, Bagnold hypothesis, entrainment, erosion, shear stress

1. Introduction

[2] Attempts to provide a mechanistic description of bed load transport under uniform equilibrium conditions have invariably fallen into one or the other of two camps, one having its origin in the work of *Einstein* [1950] and the other deriving from the work of *Bagnold* [1956].

[3] The centerpiece of the Einsteinean formulation is the specification of an entrainment rate of particles into bed load transport (pick-up function) as a function of boundary shear stress and other parameters. The work of *Nakagawa and Tsujimoto* [1980], *van Rijn* [1984], and *Tsujimoto* [1991], for example, represent formulations of this type.

[4] In the Bagnoldean formulation, however, a relation for the areal concentration of bed load particles as a function of boundary shear stress derives automatically from the imposition of a dynamic condition at the bed, according to which the fluid shear stress drops to the critical value for the onset of sediment motion. This dynamic condition is referred to here interchangeably as the Bagnold hypothesis or Bagnold constraint. The hypothesis was used by *Owen* [1964] to calculate sediment transport by saltation for the case of wind-blown sand. It is inherent in the bed load

formulations of *Ashida and Michiue* [1972] and *Engelund and Fredsoe* [1976] for nearly horizontal beds. *Wiberg and Smith* [1989], *Sekine and Kikkawa* [1992], and *Nino and Garcia* [1994a, 1994b], for example, have used the hypothesis to derive models of bed load on nearly horizontal beds based on an explicit calculation of grain saltation. *Sekine and Parker* [1992] used the Bagnold hypothesis to develop a saltation model for bed load on surface with a mild transverse slope, and *Kovacs and Parker* [1994] extended the analysis of *Ashida and Michiue* [1972] to the case of arbitrarily sloping beds. *Bridge and Bennett* [1992] have employed the Bagnold hypothesis to study the bed load transport of size mixtures.

[5] Based on the most recently published formulations of bed load transport, then, it is possible to say that the field as a whole has tended away from the Einsteinean and toward the Bagnoldean formulation. This notwithstanding, doubts have been expressed from time to time concerning the Bagnold hypothesis. For example, the experimental work of *Fernandez Luque and van Beek* [1976] does not support the Bagnold hypothesis. A reanalysis of the data and formulation presented by *Nino and Garcia* [1994a, 1994b] caused *Nino and Garcia* [1999] to cast further doubts on the hypothesis. *Kovacs and Parker* [1994] were forced to modify the hypothesis in order to obtain a well-behaved theory of bed load transport on arbitrarily sloping beds. Most recently, *Schmeekle* [1999] has provided experimental evidence, and *McEwan et al.* [1999] have provided evidence based on a numerical

---

[1]Now at Dipartimento di Ingegneria Civile, Università di Firenze, Firenze, Italy.

model suggesting that the Bagnold hypothesis yields very poor results at low transport stage.

[6] It is shown here that the straightforward extension of the Bagnold hypothesis to the case of arbitrarily sloping bed proves to be impossible. In particular, a solution for areal concentration of grains in bed load transport fails to exist for the case of transverse bed slopes beyond some modest value that is typically much smaller than the angle of repose. An alternative formulation that neither satisfies nor requires the Bagnold constraint is the subject of a companion contribution (G. Parker et al., Bedload at low Shields stress on arbitrarily sloping beds: Alternative entrainment formulation, submitted to *Water Resources Research*, 2002). The mechanistic basis for that contribution is presented below.

2. Empirical Relations of Fernandez Luque and van Beek

[7] While the emphasis of the present paper is on the structure of fluid-solid momentum exchange in the bed load layer rather than a specific bed load formulation, it will prove useful to refer to the experiments of *Fernandez Luque and van Beek* [1976] as an example. These experiments, hereinafter referred to as FLvB, were performed in a flume under equilibrium conditions. The sediment employed was as uniform as possible. Experiments were conducted with two sand sizes $D = 0.9$ mm (Sand1) and $D = 1.8$ mm (Sand2) and one gravel size $D = 3.3$ mm (Gravel), all of which had a specific gravity s of 2.64. In addition, experiments were also conducted with lightweight walnut shell grains ($D = 1.5$ mm, $s = 1.34$, Walnut) and heavyweight magnetite grains ($D = 1.8$ mm, $s = 4.58$; Magnetite). Tests on all five materials were conducted on stream-wise slope angles α of nearly 0°, 12°, 18° and 22° in the absence of a transverse slope. The transport rates studied were relatively low.

[8] The relevant parameters of the experiments can be defined as follows: q = mean volume bed load transport per unit width, τ_{fB} = mean fluid boundary shear stress at the bed (estimated as if there were no bed load layer), E_b = mean volume entrainment rate of bed grains into bed load saltation per unit bed area, D_b = mean volume deposition rate of bed load grains per unit bed area, L_s = mean saltation length, L_{step} = mean step length, i.e. the distance a particle goes before coming to rest, so that L_{step}/L_s = average number of saltations in one step, h_s = mean thickness of the saltating bed load layer, C = volume concentration of particles participating in bed load averaged over the bed load layer, ξ = mean areal concentration of bed load grains, given by the relation

$$\xi = C h_s \tag{1}$$

and V_P = magnitude of the mean velocity of the saltating grains, which is directed stream-wise in the case of the experiments of FLvB.

[9] The parameter τ_{fB} denotes the fluid boundary shear stress that would occur at the bed in the absence of a moving bed load layer. In the case of a steady, uniform rectilinear flow it can be estimated from either a friction relation such as the Moody diagram or the depth-slope (hydraulic radius-slope) product. The dimensionless Ein-

stein bed load number $\hat{q}$ and Shields number (Shields stress) τ_* can be defined as follows;

$$\hat{q} = \frac{q}{\sqrt{(s-1)gD}D} \tag{2a}$$

$$\tau_* = \frac{\tau_{fB}}{\rho(s-1)gD} \tag{2b}$$

where ρ denotes water density and g denotes the acceleration of gravity. In addition, the dimensionless bed load velocity $\hat{V}_P$, bed load entrainment rate $\hat{E}$, bed load deposition rate $\hat{D}$, areal concentration $\hat{\xi}$, saltation length $\hat{L}_s$ and step length $\hat{L}_{step}$ are defined as follows;

$$\hat{V}_P = \frac{V_P}{\sqrt{(s-1)gD}} \tag{2c}$$

$$\hat{E} = \frac{E_b}{\sqrt{(s-1)gD}} \tag{2d}$$

$$\hat{D} = \frac{D_b}{\sqrt{(s-1)gD}} \tag{2e}$$

$$\hat{\xi} = \frac{\xi}{D} \tag{2f}$$

$$\hat{L}_s = \frac{L_s}{D} \tag{2g}$$

$$\hat{L}_{step} = \frac{L_{step}}{D} \tag{2h}$$

[10] FLvB estimated a critical Shields stress τ_{*c} on a bed with an arbitrary stream-wise slope angle α (but no transverse slope) as follows;

$$\tau_{*c} = \tau_{*co} \cos\alpha \left(1 - \frac{\tan\alpha}{\mu}\right) \tag{3}$$

where τ_{*co} denotes the critical Shields stress on a nearly horizontal slope and μ denotes a static coefficient of Coulomb friction.

[11] The main empirical results of FLvB can be expressed as follows.

$$\hat{q} = 5.7 \left(\tau_* - \tau_{*c}\right)^{3/2} \tag{4a}$$

$$\hat{E} = 0.0199 \left(\tau_* - \tau_{*c}\right)^{3/2} \tag{4b}$$

$$\hat{V}_P = 11.5 \left(\sqrt{\tau_*} - 0.7\sqrt{\tau_{*c}}\right) \tag{4c}$$

$$\hat{L}_s = 16 \tag{4d}$$

The relation for entrainment rate $\hat{E}$ was actually determined by measuring the deposition rate $\hat{D}$. These two, however, must be equal for the case of equilibrium bed load transport. Equations (4a), (4b) and (4c) are compared with the actual data of FLvB in Figures 1a, 1b, and 1c, respectively. In
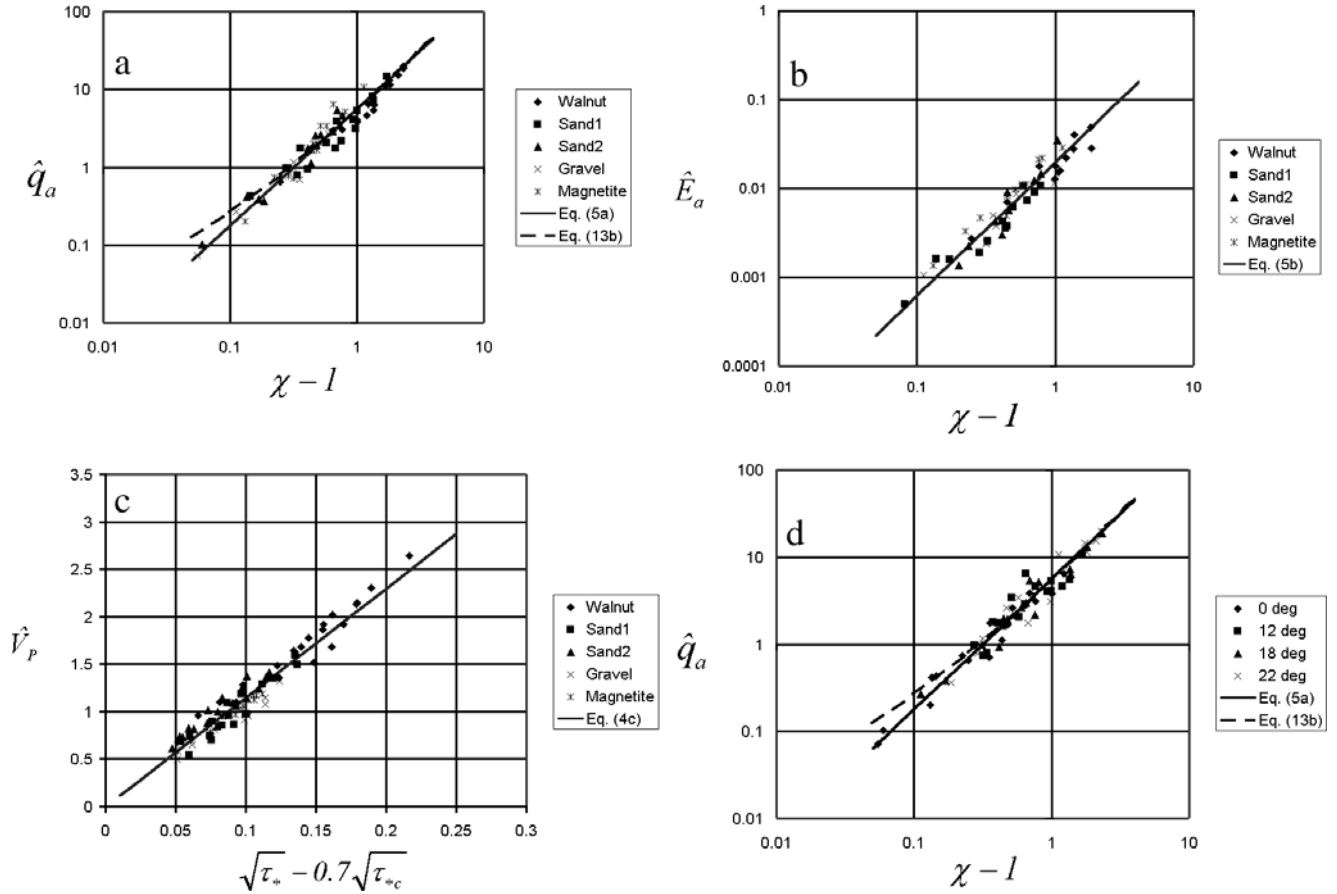
Figure 1. (a) Plot of $\hat{q}_a$ versus $\chi - 1$ for the data of FLvB, grouped according to sediment type. Also shown are (5a) and (13b). (b) Plot of $\hat{E}_a$ versus $\chi - 1$ for the data of FLvB, grouped according to sediment type. Also shown is (5b). (c) Plot of $\hat{V}_P$ versus $\sqrt{\tau_*} - 0.7\sqrt{\tau_{*c}}$ for the data of FLvB, grouped according to sediment type. Also shown is (4c). (d) Plot of $\hat{q}_a$ versus $\chi - 1$ for the data of FLvB, grouped according to bed slope. Also shown are (5a) and (13b).

Figures 1a and 1b relations (4a) and (4b) are plotted in the respective equivalent forms

$$\hat{q}_a = 5.7(\chi - 1)^{3/2} \qquad (5a)$$

$$\hat{E}_a = 0.0199(\chi - 1)^{3/2} \qquad (5b)$$

where

$$\hat{q}_a = \frac{\hat{q}}{\left(\tau_{*c}\right)^{3/2}} \qquad (5c)$$

$$\hat{E}_a = \frac{\hat{E}}{\left(\tau_{*c}\right)^{3/2}} \qquad (5d)$$

$$\chi = \frac{\tau_*}{\tau_{*c}} \qquad (5e)$$

[12] As noted above, the experiments of FLvB cover a very wide range of stream-wise bed slope angles α, spanning the range from $\alpha = 0°$ (or nearly $0°$) to $22°$. When plotted in the form of (4a), (4b) and (4c) or alternatively (5a), (5b) and (4c), into which the effect of varying slope has been folded into the parameter τ_{*c}, no other discrim-

ination of the data according to slope is readily apparent. This is shown for the case of the data for $\hat{q}_a$ versus χ in Figure 1d, in which (5a) is shown along with the data grouped according to slope.

[13] The above comment notwithstanding, it will prove of value below to analyze the data of FLvB separately for the case of a nearly horizontal bed ($\alpha = 0°$). This allows for a baseline case against which to check results obtained for an arbitrarily sloping bed. In Figure 2a their data for bed load transport over a nearly horizontal bed is compared against (5a). In Figure 2b, (5b) is compared against the data for the entrainment rate over a nearly horizontal bed. In both plots $\tau_{*c} 7 \rightarrow \tau_{*co}$ where τ_{*co} now denotes the critical Shields stress on a nearly horizontal slope and $\chi \rightarrow \tau_*/\tau_{*co}$. It is seen in both plots that the respective relations in question characterize the data well. In the work presented below, (4a), (4b) (or their respective counterparts, 5a, 5b) and (4c) are referred to as the original relations of FLvB, i.e. OFLvB for bed load, entrainment rate, and bed load velocity, respectively.

[14] Two relations describing mass conservation apply for equilibrium bed load transport;

$$q = V_P C h_s \qquad (6a)$$
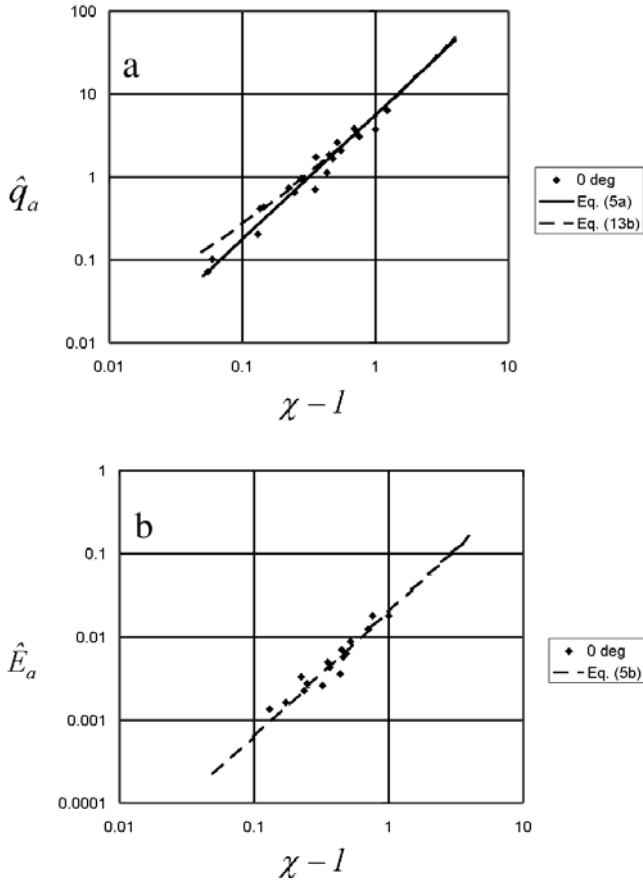
$$q = E_b L_{step} \qquad (6b)$$

Figure 2. (a) Plot of $\hat{q}_a$ versus $\chi - 1$ for only the data of FLvB, corresponding to nearly vanishing bed slope, i.e. $\alpha = 0$. Also shown are (5a) and (13b). (b) Plot of $\hat{E}_a$ versus $\chi - 1$ for only the data of FLvB, corresponding to nearly vanishing bed slope, i.e., $\alpha = 0$. Also shown is (5b).

The nondimensional forms of the above relations can be written as

$$\hat{q} = \hat{V}_P \hat{\xi} \tag{7a}$$

$$\hat{q} = \hat{E}\hat{L}_{step} \tag{7b}$$

Equations (4a), (4c) and (7b) give the evaluation

$$\hat{L}_{step} = 286 \tag{7c}$$

This value is in very close agreement with the measured value of 288, which was not found to vary with Shields stress in the experiments of FLvB. They also deduced a value for dimensionless saltation length $\hat{L}_s$ equal to 16 and again independent of Shields stress.

[15] Between (4a) and (4c) applied to nearly horizontal slopes ($\tau_{*c} = \tau_{*co}$ therein) and (7a) it is found that

$$\hat{\xi} = 0.496 \frac{\left(\tau_* - \tau_{*co}\right)^{3/2}}{\left(\sqrt{\tau_*} - 0.7\sqrt{\tau_{*co}}\right)} \tag{8}$$

It is useful to have an expression for the deposition rate D_b of bed load particles that explicitly includes particle

concentration C or alternatively ξ, so that the deposition rate vanishes when there is no sediment in saltation. Between (1), (2e), (4c), (7a), (7b), (7c), and the equilibrium condition

$$E_b = D_b \tag{9}$$

it is found that

$$\hat{D} = 0.04\left(\sqrt{\tau_*} - 0.7\sqrt{\tau_{*co}}\right)\hat{\xi} \tag{10}$$

[16] FLvB note that according to (8)$\hat{\xi}$ varies "almost linearly" in $\tau_* - \tau_{*c}$. In point of fact the approximation

$$\left(\sqrt{\tau_*} - 0.7\sqrt{\tau_{*co}}\right) \cong 0.75\left(\tau_* - \tau_{*co}\right)^{1/2} \tag{11a}$$

turns out to be accurate over all but the very lowest range of shear stresses studied by Luque and van Beek. This can be shown by defining the functions

$$f_a(\chi) = \left(\sqrt{\chi} - 0.7\right) \tag{11b}$$

$$f_b(\chi) = 0.75(\chi - 1)^{1/2} \tag{11c}$$

where in analogy to (5e)

$$\chi = \frac{\tau_*}{\tau_{*co}} \tag{11d}$$

The comparison is performed in Figure 3 over the range studied by Fernandez Luque and van Beek. The agreement is excellent in the range of interest except very near the threshold of motion.

[17] Employing the approximation (11a) in (8) the following linear expression is obtained;

$$\hat{\xi} = 0.66\left(\tau_* - \tau_{*co}\right) \tag{12}$$

The same approximation in (4a) and (10) yields the respective results

$$\hat{q} = 7.59\left(\tau_* - \tau_{*co}\right)\left(\sqrt{\tau_*} - 0.7\sqrt{\tau_{*co}}\right) \tag{13a}$$

or alternatively

$$\hat{q}_\alpha = 7.59(\chi - 1)\left(\sqrt{\chi} - 0.7\right) \tag{13b}$$

where χ is given by (11d) and

$$\hat{D} = 0.03\left(\tau_* - \tau_{*co}\right)^{1/2}\hat{\xi} \tag{14}$$

Equations (12), (13a) (as well as the alternative form 13b) and (14) are here referred to as the modified relations of FLvB, i.e. MFLvB for areal bed load concentration, bed load transport rate and deposition rate, respectively. on a nearly horizontal bed. Equation (13b) is compared against (5a) and the data of FLvB for all the data in Figure 1a and for the data corresponding to a nearly horizontal bed in Figure 2a. Again, the agreement is excellent except at very low Shields stresses.
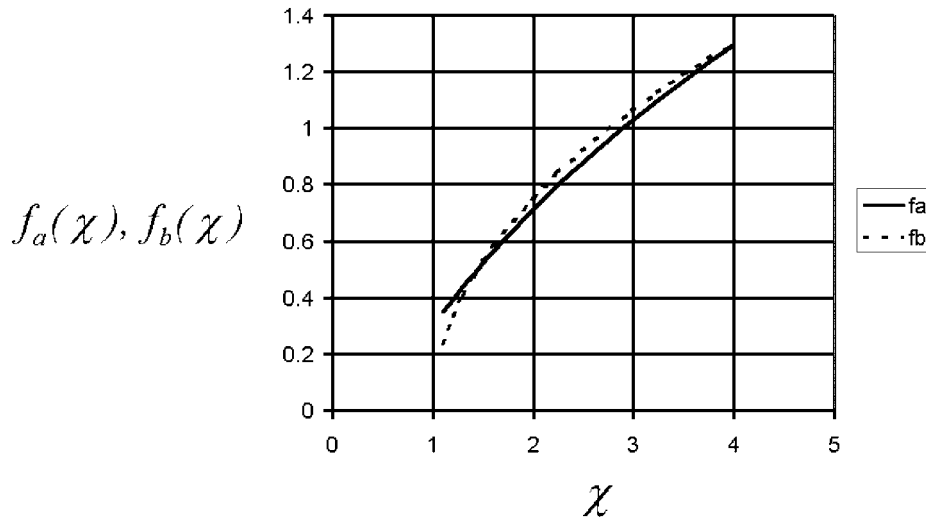
Figure 3. Plot of the functions $f_a(\chi)$ and $f_b(\chi)$ versus χ, illustrating how one may be approximated by the other.

[18] It is important to realize that both the OFLvB forms (4a), (4b), (4c), (8) and (10) and the MFLvB forms (12), (13a) and (14) fit the data accurately not only for nearly horizontal slopes, but the full range of stream-wise slopes studied by FLvB, the only necessary modification to account for finite stream-wise slope being the generalization from τ_{*co} to τ_{*c}.

[19] The OFLvB or MFLvB forms employed in the present analysis are limited to (1) those that were directly verified with data, i.e., the OFLvB forms (4a), (4b), (4c) and the MFLvB form (13a) and (2) those that could be deduced from them and general continuity relations, i.e., the OFLvB forms (8) and (10) and the MFLvB forms (12), (13) and (14). FLvB also present the important qualitative result that the Bagnold

hypothesis is not satisfied in their experiments. The means by which the deviation from the Bagnold hypothesis is computed by them, however, involves modeling assumptions as well as direct data. As a result their specific conclusions in regard to the deviation from the Bagnold hypothesis are not used in this paper. The issue is discussed in some detail in a later section.

3. Bagnold Formulation on a Nearly Horizontal Bed

[20] The Bagnoldean formulation on a nearly horizontal bed is reviewed here in the context of the exposition of
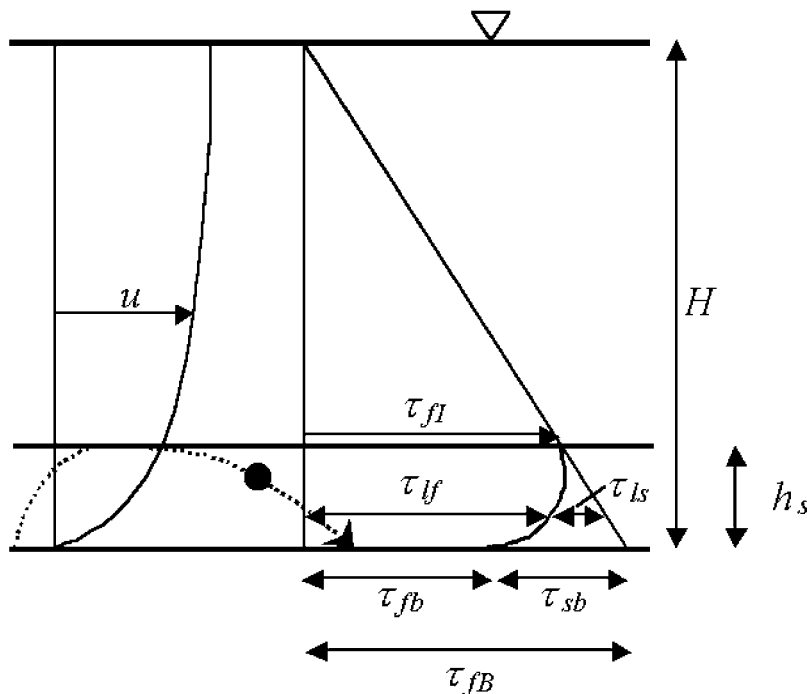

Figure 4. Definition diagram for equilibrium bed load transport on a nearly horizontal bed slope.

Ashida and Michiue [1972]; see also *Engelund and Fredsoe* [1976] for a very similar analysis. Consider the equilibrium unidirectional open channel flow over an erodible bed of Figure 4, in which x denotes the stream-wise direction and z denotes the upward normal direction. The mean flow is unidirectional and the stream-wise slope angle α is sufficiently small to allow approximating the bed as nearly horizontal with bed slope $S = \tan\alpha \ll 1$. The depth H of flow is assumed to be large compared to the thickness of the saltation layer h_s, which is in turn assumed to be at least a few grain diameters in thickness. The volume concentration of particles within the bed load layer is assumed to be small. The fluid shear stress at the interface between the bed load layer and the clear water above is denoted as τ_{fI}, as shown in Figure 4. Also shown in Figure 4 is the fluid shear stress at the bed τ_{fb}, and the shear stress of the solid phase at the bed τ_{sb}, which is realized by means of momentum transfer through oblique particle collision with the bed. All particles are assumed to be spherical with diameter D.

[21] The fluid shear stress τ_{fB} at the bed in the absence of a bed load layer is given by the relation

$$\tau_{fB} = \tau_{fI} + \rho g h_s S \qquad (15)$$

It can be expected, however, that the actual fluid shear stress τ_{fb} realized at the bed in the presence of a saltating bed load layer will be reduced below τ_{fB} due to the transfer of fluid phase momentum to solid phase momentum via drag. The momentum so transferred by drag is exported by means of oblique particle collision with the bed, giving rise to the solid phase boundary shear stress τ_{sb}.

[22] The vectorial drag force $\boldsymbol{F}_D$ on an individual particle in saltation can be written as

$$\boldsymbol{F}_D = \frac{1}{2}\rho c_D \pi \frac{D^2}{4}|\boldsymbol{u} - \boldsymbol{v}|(\boldsymbol{u} - \boldsymbol{v}) \qquad (16a)$$

where $\boldsymbol{u}$ denotes the local vectorial mean velocity of the fluid phase at level z, $\boldsymbol{v}$ denotes the corresponding vectorial velocity of the solid phase and c_D denotes the drag coefficient of the particle. This drag force can be used to compute the vectorial rate of transfer of momentum per unit volume per unit time from the fluid phase to the solid phase $\boldsymbol{t}_{fs}$;

$$\boldsymbol{t}_{fs} = \frac{\boldsymbol{F}_D}{\frac{4}{3}\pi\left(\frac{D}{2}\right)^3} c = \rho \frac{3c_D}{4D}|\boldsymbol{u} - \boldsymbol{v}|(\boldsymbol{u} - \boldsymbol{v})c \qquad (16b)$$

where c denotes the local mean volume bed load concentration at level z.

[23] Stream-wise momentum balance within the bed load layer can be considered in terms of two phases, fluid and solid. Where $\tau_{lf}(z)$ denotes the local mean stream-wise fluid shear stress at any distance z above the bed, average stream-wise momentum balance of the fluid phase requires that

$$0 = \frac{\partial \tau_{lf}}{\partial z} + \rho g S - t_{fsx} \qquad (17)$$

where t_{fsx} denotes the stream-wise component of $\boldsymbol{t}_{fs}$. The first term on the right-hand side of (17) describes the downward transfer of stream-wise fluid momentum by

(predominantly) turbulent diffusion. The second term describes the force of gravity on the fluid in the bed load layer. The third term describes the rate of transfer of stream-wise fluid momentum to the solid phase via drag.

[24] The corresponding stream-wise momentum balance for the solid phase can be written as

$$0 = \frac{\partial \tau_{ls}}{\partial z} + \rho(s - 1)cgS + t_{fsx} \qquad (18a)$$

where τ_{ls} denotes the local mean shear stress of the solid phase, which may be estimated by the relation

$$\tau_{ls} = -\rho s(c_u v_{xu} v_{zu} + c_d v_{xd} v_{zd}) \qquad (18b)$$

where the subscript u refers to upward-moving bed load particles and the subscript d refers to downward-moving bed load particles [e.g. *Owen*, 1964]. The first term on the right-hand side of (18a) describes the net downward rate of transfer of stream-wise momentum by saltating particles. The second term accounts for the stream-wise force of gravity on the solid phase. The third term describes the rate of transfer of stream-wise momentum from the fluid phase to the solid phase by drag.

[25] Momentum balance of the solid phase in the upward normal direction can be quantified as

$$0 = \rho(s - 1)cg - \frac{\partial p_{ls}}{\partial z} + t_{fsz} \qquad (19a)$$

where p_{ls} denotes the local mean pressure (or the negative of the normal stress) of the solid phase, which may be estimated as

$$p_{ls} = \rho s\left(c_u v_{zu}^2 + c_d v_{zd}^2\right) \qquad (19b)$$

[e.g., *Owen*, 1964]. The first term on the right-hand side of (19a) quantifies the submerged weight per unit volume of the bed load particles, the second term quantifies the solid-phase momentum transfer rate in the upward normal direction and the final term t_{fsz} denotes the upward normal component of the drag transfer term $\boldsymbol{t}_{fs}$.

[26] Equations (17), (18a) and (19a) are now integrated over the bed load layer subject to the following boundary conditions;

$$\tau_{lf}\big|_{z=h} = \tau_{fI} \qquad (20a)$$

$$\tau_{ls}\big|_{z=h} = 0 \qquad (20b)$$

$$p_{ls}\big|_{z=h} = 0 \qquad (20c)$$

and the definitions

$$\tau_{lf}\big|_{z=o} \equiv \tau_{fb} \qquad (20d)$$

$$\tau_{ls}\big|_{z=o} \equiv \tau_{sb} \qquad (20e)$$

$$p_{ls}\big|_{z=0} \equiv p_{sb} \qquad (20f)$$

In performing the integration the drag terms t_{fsx} and t_{fsz} are integrated approximately to yield the evaluations

$$\int_0^{h_s} t_{fsx} dz \cong T_{fsx} h_s \qquad (21a)$$

$$T_{fsx} = \rho \frac{3c_D}{4D}(U - V_P)^2 C \qquad (21b)$$

$$\int_0^{h_s} t_{fsz} dz \cong 0 \qquad (21c)$$

where U and V_P denote the magnitudes of the layer-averaged stream-wise velocities of the fluid and solid phases, respectively, and C denotes the layer-averaged bed load concentration. The integral of (21c) is approximated as vanishing because in an equilibrium bed load layer the upward normal components of both the fluid and particle velocities should average to zero.

[27] Performing the integrations with aid of (1), (20) and (21), it is found that

$$0 = \tau_{fI} - \tau_{fb} + \rho h_s g S - \rho \frac{3c_D}{4D}\xi(U - V_P)^2 \qquad (22)$$

$$0 = -\tau_{sb} + \rho(s - 1)\xi g S + \rho \frac{3c_D}{4D}\xi(U - V_P)^2 \qquad (23)$$

$$0 = p_{sb} - \rho(s - 1)g\xi \qquad (24)$$

[28] Equations (22) and (23) may be summed and reduced with (15) to yield the following result;

$$\tau_{fB} + \rho(s - 1)g\xi S = \tau_{fb} + \tau_{sb} \qquad (25a)$$

In the limit of a nearly horizontal bed (25a) accurately approximates to

$$\tau_{fB} = \tau_{fb} + \tau_{sb} \qquad (25b)$$

That is, the fluid shear stress τ_{fB} that would prevail at the bed in the absence of a bed load layer is partitioned between a) the actual fluid shear stress at the bed τ_{fb} in the presence of a bed load layer and b) the stress at the bed due to the solid phase τ_{sb}.

[29] The Bagnoldean formulation employs two assumptions to close the above equations. The first is the introduction of an order-one dynamic coefficient of Coulomb friction μ_{do} (the subscript "o" denoting the value for a nearly horizontal bed) relating the normal and shear stresses of the solid phase;

$$\tau_{sb} = \mu_{do} p_{sb} \qquad (26)$$

Equation (26) may be used to characterize the mean velocity of bed load particles as outlined below.

[30] Between (23), (24), (25b) and (26) and the assumption of a nearly horizontal bed ($S \ll 1$) it is found that

$$0 = -\mu_{d0}(s - 1)g + \frac{3c_D}{4D}(U - V_P)^2 \qquad (27a)$$

$$\tau_{fB} - \tau_{fb} = \mu_{do}\rho(s - 1)g\xi \qquad (27b)$$

A shear velocity u_τ can be defined as follows;

$$u_\tau = \sqrt{\frac{\tau_{fB}}{\rho}} \qquad (28)$$

In the present analysis the effective layer-averaged stream-wise flow velocity U acting on the saltating bed load layer is related to the shear velocity u_τ according to the form

$$\frac{U}{u_\tau} = f \qquad (29)$$

where in classical treatments f is related to the ratio h_s/D according to an application of the logarithmic law of the wall just above the bed load layer [e.g., *Ashida and Michiue*, 1972]. In the limit at which grain saltation ceases $V_P \to 0$, in which case (27)–(29) yield a critical Shields stress for the cessation of saltation on a nearly horizontal bed τ_{*cso};

$$\tau_{*cso} = \frac{4\mu_{do}}{3c_D f^2} \qquad (30)$$

In general this parameter is found to be less than the critical Shields stress for the initiation of motion τ_{*co} on a nearly horizontal bed. This is partly because the parameters μ_{do}, c_D and f that apply to a moving particle that is near the condition for the cessation of motion are somewhat different from those that apply to a particle at rest that is about to move. A more significant reason for the difference, however, is related to the fact that a particle, once dislodged, typically must undergo a number of saltations before it finds a spot on the bed with a microstructure that allows it to stop again. FLvB determined the following relation on semiempirical grounds:

$$\tau_{*cso} = \lambda_o^2 \tau_{*co} \qquad (31)$$

where $\lambda_o < 1$ is an order-one constant that they found to be equal to 0.7. The subscript "o" in λ_o denotes the value for a nearly horizontal bed.

[31] Equation (27a) may now be solved for particle velocity with the aid of (30) and (31) and reduced to the dimensionless forms of (2b) and (2c), resulting in the expression

$$\hat{V}_P = f\left(\sqrt{\tau_*} - \lambda_o\sqrt{\tau_{*co}}\right) \qquad (32)$$

for particle velocity as a function of Shields stress.

[32] The second and more crucial assumption is the Bagnold constraint itself. It is assumed that under equilibrium conditions the fluid shear stress at the bed τ_{fb} becomes equal to the critical value τ_{fco} for the onset of particle motion, the subscript "o" again denoting a horizontal bed;

$$\tau_{fb} = \tau_{fco} \qquad (33)$$

[33] Equation (33) combined with (27b) yields a specific predictive relation for the areal concentration of bed load particles;

$$\hat{\xi} = \frac{1}{\mu_{do}}\left(\tau_* - \tau_{*co}\right) \qquad (34)$$

where

$$\tau_{*co} = \frac{\tau_{fco}}{\rho(s-1)gD} \qquad (35)$$

[34] The above results can be applied directly to the experiments of FLvB, which encompass results for a nearly horizontal bed ($\alpha = 0°$). Choosing $f = 11.5$ and $\lambda_o = 0.7$ reduces (32) to the OFLvB form (4c) for particle velocity. In addition, with the additional choice $\mu_{do} = 1.515$ (34) reduces to the MFLvB form (12) for areal concentration of bed load, and (32) and (34) combined with the continuity relation (7a) reduce to the MFLvB form (13a) based for bed load transport.

[35] The part of the above formulation that is crucially dependent upon the Bagnold hypothesis is the relation for dimensionless areal concentration $\hat{\xi}$ as a function of Shields stress τ_*. The above analysis appears to be both reasonable and justified by the data of FLvB with the one exception that the deduced value of μ_{do} of 1.515 appears to be unrealistically high. Specifically, it corresponds to a dynamic friction angle of 56.6°, i.e. well above the angle of repose for any natural sediment. This value also appears to be very high when compared with the values deduced by *Abbott and Francis* [1977], *Ashida and Michiue* [1972], *Wiberg and Smith* [1985], *Sekine and Kikkawa* [1992], and *Nino and Garcia* [1994a, 1994b]. In addition, *Bagnold* [1973] himself argues that μ_{do} should not exceed μ, which he estimates as 0.63, corresponding to an angle of repose ϕ_r of about 32°. The study of *Nino and Garcia* [1994b] indicates a value close to 0.3 that has little tendency to vary with Shields stress τ_*.

[36] The observation that the value of μ_{do} necessary to reconcile the Bagnold hypothesis with the data of FlvB is unrealistically high is in and of itself a strong reason to doubt the validity of the hypothesis. In addition, it presages a far more convincing reason to reject the hypothesis. The good agreement obtained above with the use of the Bagnold constraint and the value μ_{do} of 1.515 is an illusion. As is demonstrated below, the Bagnold hypothesis fails to yield a solution when applied to equilibrium bed load over a bed with a transverse slope that is in excess of values that are well below the angle of repose. It thus cannot be correct, even for the case of a nearly horizontal bed.

4. Threshold Condition for the Onset of Motion on an Arbitrarily Sloping Bed

[37] As was seen above, the Bagnold hypothesis states that under conditions of equilibrium bed load transport the fluid shear stress at the bed must drop to the critical value at the threshold of motion. In order to test the hypothesis on arbitrarily sloping beds, then, it is necessary to have at hand a generalized formulation for the threshold of motion for that case. A partial generalization has already been presented, i.e. (3), which applies to arbitrary slopes in the stream-wise direction. The formulation is generalized below to the case of transverse slopes as well.

[38] The analysis presented below follows the approach of *Kovacs and Parker* [1994], but with the inclusion of the effect of fluid lift, which was omitted from that analysis. Consider free surface flow over a plane but arbitrarily tilted cohesionless granular surface consisting of uniform particles of size D, as shown in Figure 5. Let P denote a point
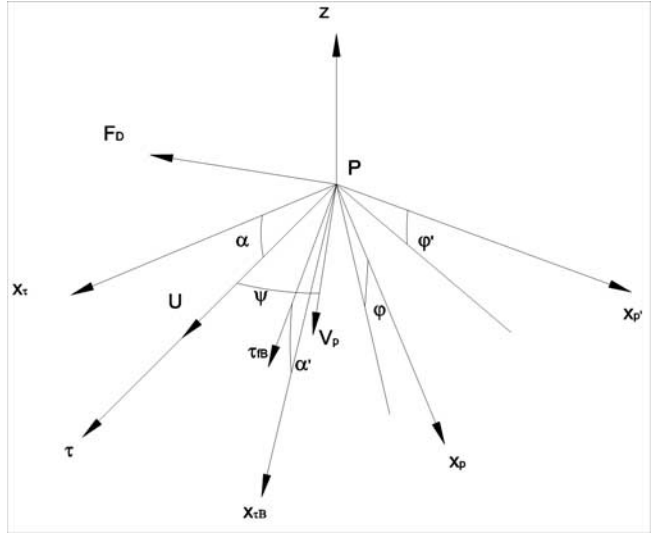

Figure 5. Definition diagram for bed load transport on an arbitrarily sloping bed.

on the bed and let z now be the coordinate of an upward vertical axis with origin at P and unit directional vector $\hat{k}$. The flow exerts a tangential shear stress τ_{fB} on the bed. Here τ_{fB} represents a vectorial generalization of the scalar parameter τ_{fB} presented above, and quantifies the shear stress that would be applied to the bed in the absence of a bed load layer. The direction of this shear stress vector and the vertical direction, provide the only two externally imposed directions on the problem. It is thus convenient to introduce a right-handed Cartesian reference frame centered at P, with coordinates x_τ, x_p and z. The x_τ axis, which has unit vector $\hat{x}_\tau$, is the horizontal axis lying in the vertical plane $(\boldsymbol{\tau_{fB}}, \hat{k})$, while the x_p axis, which has unit vector $\hat{x}_p$, is the horizontal axis orthogonal to the plane $(\hat{x}_\tau, \hat{k})$.

[39] The equation of the bed surface maybe written in the form

$$F_b = z - \eta(x_\tau, x_p) = 0 \qquad (36)$$

where η denotes bed elevation. The unit vector upward normal to the bed takes the form

$$\hat{n} = \frac{\nabla F_b}{|\nabla F_b|} \qquad (37)$$

The unit downward vertical vector - $\hat{k}$ is decomposed into a normal component $\hat{k}_n$ and a tangential component $\hat{k}_t$ as follows;

$$\boldsymbol{k}_n = (-\hat{k} \cdot \hat{n})\hat{n} \qquad (38a)$$

$$\boldsymbol{k}_t = -\hat{k} - \boldsymbol{k}_n \qquad (38b)$$

The stream-wise slope angle α of the bed a point P is then defined as the slope of the line resulting from the intersection of the bed surface with the plane $(\hat{k}, \hat{x}_\tau)$;

$$\tan \alpha = -\frac{\partial \eta}{\partial x_\tau} \qquad (39)$$

The corresponding transverse slope angle φ of the bed at P is similarly defined as the slope of the line resulting from

the intersection of the bed surface with the plane $(\hat{k}, \hat{x}_p)$;

$$\tan\varphi = -\frac{\partial\eta}{\partial x_p} \qquad (40)$$

Note that these two lines are not in general orthogonal to each other.

[40] The treatment of forces on a particle at the threshold of motion used here represents a vectorial generalization of the treatment of *Ikeda* [1982], which was originally formulated for a ''dangerously'' placed particle on a nearly horizontal bed. The drag force $\boldsymbol{F}_D$, lift force $\boldsymbol{F}_L$ and submerged gravitational force $\boldsymbol{G}_s$ are given by the relations

$$\boldsymbol{F}_D = F_D\hat{\boldsymbol{s}} \qquad (41a)$$

$$F_D = \frac{1}{2}\rho c_D \frac{\pi D^2}{4} U^2 \qquad (41b)$$

$$\boldsymbol{F}_L = F_L\hat{\boldsymbol{n}} \qquad (41c)$$

$$F_L = \rho\frac{4}{3}\frac{\pi D^3}{8}c_L U^2 \left(\frac{1}{f}\left.\frac{df}{d\varsigma}\right|_{\varsigma_p}\right) \qquad (41d)$$

$$\boldsymbol{G}_s = G_s\hat{\boldsymbol{k}} \qquad (41e)$$

$$G_s = \rho(s-1)g\frac{4}{3}\frac{\pi D^3}{8} \qquad (41f)$$

In the above relations $\hat{s}$ denotes a unit vector corresponding to the direction of $\boldsymbol{\tau}_{fB}$, ζ denotes an upward normal coordinate from the bed, U denotes the magnitude of the tangential fluid velocity $\boldsymbol{U}$ at an upward distance ζ_p from the mean bed corresponding to the centroid of the ''dangerously'' placed particle, c_D and c_L are drag and lift coefficients and the parameter f, defined analogously to (29), defines the variation of U in the upward normal direction as follows;

$$\frac{U}{u_\tau} = f \qquad (42a)$$

$$u_\tau = \sqrt{\frac{|\boldsymbol{\tau}_{fB}|}{\rho}} \qquad (42b)$$

In practice f can be specified in terms of the logarithmic law of the wall, which can be written in the general form

$$f = \frac{1}{\kappa}\ell n\left(B\frac{\varsigma}{k_s}\right) \qquad (43a)$$

where $\kappa = 0.4$ is the Karman constant, k_s is a roughness height typically specified as

$$k_s = n_k D \qquad (43b)$$

and n_k is an order-one constant. In addition B is a function of friction Reynolds number $u_\tau k_s/\nu$ where ν denotes the kinematic viscosity of water. In the case for which $u_\tau k_s/\nu$ is sufficiently large B obtains the limiting value of 30 corresponding to a rough turbulent wall flow.
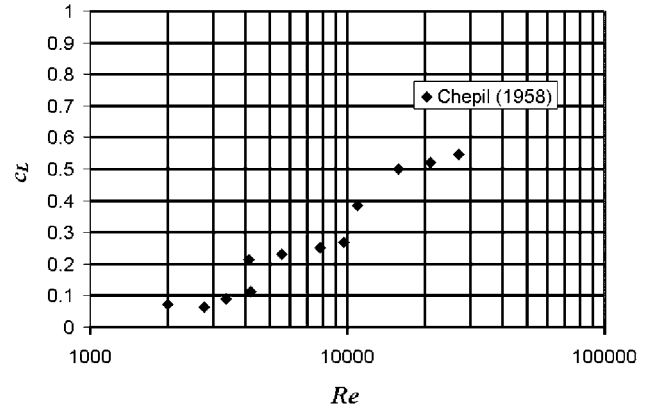

Figure 6. Plot of c_L versus Reynolds number *Re*. the data are those of *Chepil* [1958].

[41] The form employed here for fluid lift, (41d), is somewhat different from previous forms, and thus deserves some elaboration. The turbulent hydrodynamic processes which determine the average fluid forces acting on spheres lying on granular beds are far too complex to be amenable to a rigorous theoretical investigation. This notwithstanding, considerable progress has been made in the last two decades. In particular, *Auton* [1987] has shown that when the strength of vorticity is weak, i.e. when the change in incident velocity across the sphere is much smaller than the relative speed of the ambient flow along a tangent passing through the center of the sphere, the lift force $\boldsymbol{F}_L$ acting on a sphere at rest in a weakly rotational inviscid flow is given by the expression

$$\boldsymbol{F}_L = -\rho c_L \boldsymbol{u}_o x \omega \qquad (44)$$

where $\boldsymbol{u}_o$ is the flow velocity vector acting on the centroid of the particle, ω denotes a uniform ambient vorticity and c_L takes the value 0.5.

[42] The above form was shown by *Auton et al.* [1988] to also apply to the case for which the ambient flow is also slowly varying in space and time. A sphere lying on a cohesionless granular bed is subject to strongly rather than weakly sheared ambient flow. In addition, the presence of the bed and viscous effects also probably play a non-negligible role. This notwithstanding, the form of (44) is the most reasonable general form that might be envisaged for the lift force. In the present case of a particle near a wall (44) reduces to (41d).

[43] Here c_L has been estimated by reinterpreting the work of *Chepil* [1958] on the lift force acting on spheres on a granular bed in terms of (41d). The result of such a reinterpretation is shown in Figure 6. Therein it is seen that c_L increases with Reynolds number, approaching the value of 0.5 appropriate to weakly sheared, unbounded inviscid flows at large Reynolds number.

[44] It is worth mentioning that the formulation proposed for the lift force by *Wiberg and Smith* [1985] reduces to the present formulation if the velocity distribution of the incident flow is assumed to vary linearly across the sphere.

[45] The condition for incipient particle motion is one such that the impelling tangential force, i.e. the sum of drag and the downslope component of the gravitational force is

just balanced by the tangential Coulomb resistive force, which is represented in terms of the product of a static Coulomb resistance coefficient μ times the net downward normal force associated with gravity and lift. Since the Coulomb resistive force by definition opposes the direction of the impelling force, the resulting balance can be represented in terms of force magnitudes;

$$|F_D \hat{s} + G_s \boldsymbol{k}_t| = \mu|G_s \boldsymbol{k}_n + F_L \hat{\boldsymbol{n}}| \tag{45}$$

[46] The above relation can be placed in explicit form with the use of the following relationships;

$$\hat{\boldsymbol{n}} = \frac{(\tan\alpha, \tan\varphi, 1)}{\sqrt{1 + \tan^2\alpha + \tan^2\varphi}} \tag{46a}$$

$$\hat{\boldsymbol{k}} = (0, 0, 1) \tag{46b}$$

$$\boldsymbol{k}_n = -\frac{(\tan\alpha, \tan\varphi, 1)}{1 + \tan^2\alpha + \tan^2\varphi} \tag{46c}$$

$$\boldsymbol{k}_t = \frac{(\tan\alpha, \tan\varphi, -\tan^2\alpha - \tan^2\varphi)}{1 + \tan^2\alpha + \tan^2\varphi} \tag{46d}$$

$$\hat{\boldsymbol{s}} = (\cos\alpha, 0, -\sin\alpha) \tag{47}$$

Substituting (41) and (45)–(47) into (44), using (42b) to compute the value of the magnitude of the critical shear stress τ_{fc} and reducing with the definitions

$$\tau_{*c} = \frac{\tau_{fc}}{\rho(s-1)gD} \tag{48a}$$

$$\tau_{*co} = \tau_{*c}\big|_{\alpha=0, \varphi=0} \tag{48b}$$

the following algebraic relation for the ratio τ_{*c}/τ_{*co} is obtained;

$$(1-\Delta)\left(\frac{\tau_{*c}}{\tau_{*co}}\right)^2 + 2\left\{\frac{\Delta}{\sqrt{1 + \tan^2\alpha + \tan^2\varphi}} + \frac{\sin\alpha}{\mu}\right\}\left(\frac{\tau_{*c}}{\tau_{*co}}\right)$$

$$+ \frac{(1+\Delta)}{1 + \tan^2\alpha + \tan^2\varphi}\left(-1 + \frac{\tan^2\alpha + \tan^2\varphi}{\mu^2}\right) = 0 \tag{49}$$

where the critical Shields stress on a horizontal bed τ_{*co} is given by the relation

$$\tau_{*co} = \frac{4\mu}{3c_D f^2|_{\varsigma_p}(1+\Delta)} \tag{50}$$

and Δ is a parameter quantifying the effect of the lift force, given by

$$\Delta = \frac{4}{3}\mu\frac{c_L}{c_D}r_L \tag{51a}$$

$$r_L = \left(\frac{D}{f}\frac{df}{d\varsigma}\right)\bigg|_{\varsigma_p} = \frac{1}{\frac{\varsigma_p}{D}\ell n\left(B\frac{\varsigma_p}{n_k D}\right)} \tag{51b}$$
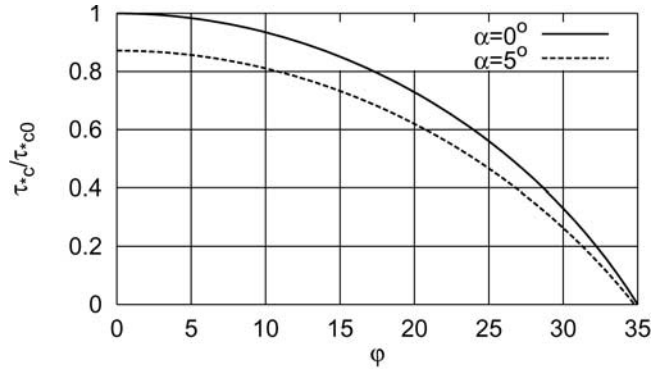

Figure 7. Plot of the ratio τ_{*c}/τ_{*co} as a function of transverse angle φ for two stream-wise angles α. In the calculations $\tan^{-1}(\mu) = 35°$, $f = 6.81$, $c_L/c_D = 0.85$, and $r_L = 0.74$.

[47] It is of value to point out some limiting cases of (49). In the limiting case of a horizontal bed the expected result is obtained;

$$\tau_{*c}\big|_{\alpha=0, \varphi=0} = \tau_{*co} \tag{52a}$$

In the limiting case of a bed that is tilted only in the stream-wise direction, the relation (3) used by FLvB is recovered;

$$\tau_{*c}\big|_{\varphi=0} = \tau_{*co}\cos\alpha\left(1 - \frac{\tan\alpha}{\mu}\right) \tag{52b}$$

In the limiting case of a bed that is tilted only in the transverse direction, it is found that

$$\tau_{*c}\big|_{\varphi=0} = \tau_{*co}\cos\varphi\frac{\left\{\left[1 - (1-\Delta)^2\frac{\tan^2\varphi}{\mu^2}\right]^{1/2} - \Delta\right\}}{1-\Delta} \tag{52c}$$

The above result reduces to the familiar form specified by *Graf* [1971] if the effect of lift is neglected, so that $\Delta = 0$;

$$\tau_{*c}\big|_{\varphi=0} = \tau_{*co}\cos\varphi\left(1 - \frac{\tan^2\varphi}{\mu^2}\right)^{1/2} \tag{52d}$$

In all cases τ_{*c} drops to zero when the bed slope attains the angle of repose ϕ_r, where

$$\tan\phi_r = \mu \tag{53}$$

[48] The quadratic form (49) is easily solved for an arbitrarily sloping bed. Sample calculations are shown in Figure 7, in which the evaluations $\phi_r = \tan^{-1}(\mu) = 35°$, $c_L/c_D = 0.85$, $f = 6.81$ (corresponding to $\xi_p = 0.5$ and $n_k = 1$ in equations 43a and 43b) and $r_L = 0.74$ have been used, resulting in the value $\tau_{*co} = 0.034$.

5. Direction and Magnitude of Particle Velocity on an Arbitrarily Sloping Bed

[49] In this section the analysis that led to (32) describing the mean velocity of saltating particles over a nearly horizontal bed is generalized to an arbitrarily sloping bed. The direct generalizations to (22), (23) and (24) on an arbitrarily sloping bed are, respectively,

$$0 = \tau_{fI} - \tau_{fb} + \rho h_s g \boldsymbol{k}_t - \rho \frac{3 c_D}{4D} \xi |\boldsymbol{U} - \boldsymbol{V}_P|(\boldsymbol{U} - \boldsymbol{V}_P) \quad (54)$$

$$0 = -\boldsymbol{\tau}_{sb} + \rho(s-1)\xi g \boldsymbol{k}_t + \rho \frac{3 c_D}{4D} \xi |\boldsymbol{U} - \boldsymbol{V}_P|(\boldsymbol{U} - \boldsymbol{V}_P) \quad (55)$$

$$0 = p_{sb} - \rho(s-1)g \xi |\boldsymbol{k}_n| \quad (56)$$

In the above relations $\boldsymbol{U}$ and $\boldsymbol{V}_P$ denote the vectors of mean tangential fluid and particle velocities in the bed load layer. The corresponding generalization of (26) is

$$\boldsymbol{\tau}_{sb} = \mu_d p_{sb} = \mu_d \rho(s-1)g \xi |\boldsymbol{k}_n| \frac{\boldsymbol{V}_P}{|\boldsymbol{V}_P|} \quad (57a)$$

where $\hat{\boldsymbol{s}}_p$ denotes a unit vector in the direction of particle motion, given by

$$\hat{\boldsymbol{s}}_p = \frac{\boldsymbol{V}_P}{|\boldsymbol{V}_P|} \quad (57b)$$

and the dynamic coefficient of friction μ_d on a sloping bed may in general differ somewhat from the value μ_{do} on a nearly horizontal bed.

[50] Adding (54) and (55), it is found that

$$\boldsymbol{\tau}_{fB} = \boldsymbol{\tau}_{fb} + \boldsymbol{\tau}_{sb} + \rho(s-1)\xi g \boldsymbol{k}_t \quad (58)$$

where $\boldsymbol{\tau}_{fB}$ represents the fluid shear stress at the bed that would prevail in the absence of a bed load layer, given by

$$\boldsymbol{\tau}_{fB} = \boldsymbol{\tau}_{fI} + \rho g h_s \boldsymbol{k}_t \quad (59)$$

Here (57), (58) and (59) are the vectorial analogs of (26), (25a) and (15), respectively.

[51] The following relation for particle velocity $\boldsymbol{V}_P$ results from (55) and (57);

$$0 = -\mu_d(s-1)g|\boldsymbol{k}_n|\hat{\boldsymbol{s}}_p + (s-1)g\boldsymbol{k}_t + \frac{3 c_D}{4D}|\boldsymbol{U} - \boldsymbol{V}_P|(\boldsymbol{U} - \boldsymbol{V}_P) \quad (60)$$

The closure assumption of (29) is generalized to

$$\boldsymbol{U} = U\hat{\boldsymbol{s}} \quad (61a)$$

$$\boldsymbol{\tau}_{fB} = \tau_{fB}\hat{\boldsymbol{s}} \quad (61b)$$

$$u_\tau = \sqrt{\frac{\tau_{fB}}{\rho}} \quad (61c)$$

$$\frac{U}{u_\tau} = f \quad (61d)$$

where f is again determined from the logarithmic law of the wall. Reducing (60) with (2b), (2c), (30), (61) and a generalized form of (31) for a tilted bed, it is found that

$$\left| \sqrt{\tau_*}\hat{\boldsymbol{s}} - \frac{\hat{V}_P}{f}\hat{\boldsymbol{s}}_p \right| \left(\sqrt{\tau_*}\hat{\boldsymbol{s}} - \frac{\hat{V}_P}{f}\hat{\boldsymbol{s}}_p \right) = \lambda^2 \tau_{*co}\left(|\boldsymbol{k}_n|\hat{\boldsymbol{s}}_p - \frac{\boldsymbol{k}_t}{\mu_d} \right) \quad (62)$$

where λ is the generalization of the parameter λ_o to the case of a tilted bed, so as to include the possibility that $\lambda \neq \lambda_o$ when the bed is not horizontal or nearly so, and

$$\hat{V}_P = \frac{V_P}{\sqrt{(s-1)gD}} \quad (63a)$$

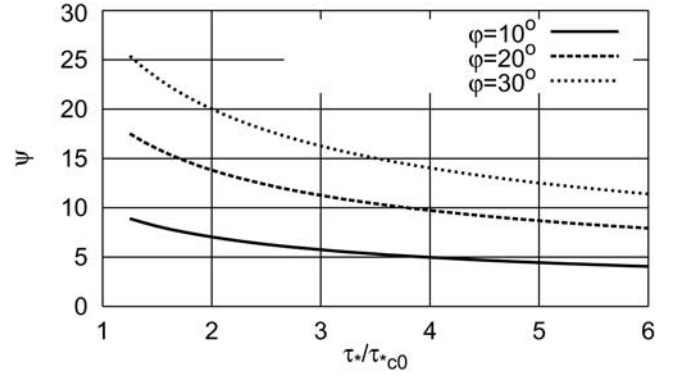**Figure 8.** Plot of the angle ψ as a function of the ratio τ_{*c}/τ_{*co} for three transverse angles φ and the stream-wise angle $\alpha = 0$. In the calculations $\lambda = 0.7, f = 11.5$, and $\tau_{*co} = 0$.

$$V_P = |\boldsymbol{V}_P| \quad (63b)$$

$$\tau_* = \frac{\tau_{fB}}{\rho(s-1)gD} \quad (63c)$$

[52] Once the direction of the applied shear stress $\hat{\boldsymbol{s}}$, the Shields stress magnitude τ_*, the directional vectors $\boldsymbol{k}_n$ and $\boldsymbol{k}_t$, the critical Shields stress τ_{*co}, the dynamic coefficient of Coulomb friction μ_d and the parameters f and λ are supplied, (62) may be solved iteratively for both the magnitude of the particle velocity $\hat{V}_P$ and the particle direction $\hat{\boldsymbol{s}}_p$. Note that in the case of one dimensional flow over a horizontal bed ($\hat{\boldsymbol{s}} \times \hat{\boldsymbol{s}}_p = 0$, $|\boldsymbol{k}_n| = 1$, $\boldsymbol{k}_t = 0$) (32) is recovered. The further specifications $f = 11.5$ and $\lambda = \lambda_o = 0.7$ recover the OFLvB relation (4c) applied to a nearly horizontal bed.

[53] In general the direction of particle motion $\hat{\boldsymbol{s}}_p$ does not coincide with the direction of applied shear stress $\hat{\boldsymbol{s}}$ unless the bed has no transverse tilt. In order to illustrate this let ψ denote the angle between particle direction $\hat{\boldsymbol{s}}_p$ and the direction of applied shear stress $\hat{\boldsymbol{s}}$, such that

$$\cos \psi = \hat{\boldsymbol{s}}_p \cdot \hat{\boldsymbol{s}} \quad (64)$$

The particle velocity vector can then be represented as

$$\boldsymbol{V}_P = V_P \cos \psi \, \hat{\boldsymbol{s}} + V_P \sin \psi (\hat{\boldsymbol{n}} \times \hat{\boldsymbol{s}}) \quad (65)$$

Recalling (47) and noting that

$$\hat{\boldsymbol{n}} \times \hat{\boldsymbol{s}} = \frac{\left(-\sin \alpha \tan \varphi, \frac{1}{\cos \alpha}, -\cos \alpha \tan \varphi \right)}{\sqrt{1 + \tan^2 \alpha + \tan^2 \varphi}} \quad (66)$$

it becomes possible to project (62) into the directions $\hat{\boldsymbol{s}}$ and $\hat{\boldsymbol{n}} \times \hat{\boldsymbol{s}}$. This allows the derivation of two scalar relationships for $\hat{V}_P$ and ψ. These can be written as

$$\hat{V}_P = f \sqrt{\tau_*} A(\psi, \alpha, \varphi) \quad (67a)$$

and

$$\sqrt{\tau_*} = \lambda \sqrt{\tau_{*co}} \frac{\left(\frac{\cos \alpha \tan \varphi}{\mu_d} - \sin \psi \right)^{1/2}}{[(1 + A'^2)(1 + \tan^2 \alpha + \tan^2 \varphi)]^{1/4}} \left(A' + \frac{1}{\tan \psi} \right) \quad (67b)$$

where the functional relations for A and A' are specified as

$$A = (\cos\psi + A'\sin\psi)^{-1} \tag{68a}$$

$$A' = \frac{\mu_d \cos\psi - \sin\alpha\sqrt{1 + \tan^2\alpha + \tan^2\varphi}}{\cos\alpha\tan\varphi - \mu_d\sin\psi} \tag{68b}$$

[54] The relations (67a) and (67b) must be solved iteratively for $\hat{V}_P$ and ψ once the parameters τ_{*co}, τ_*, f, λ, μ_d, α and φ are specified. A sample evaluation of ψ as a function of τ_* and φ is given in Figure 8 for the case $\alpha = 0$, $\lambda = 0.7$, $f = 11.5$ and $\tau_{*co} = 0.04$. As can be seen therein the angle ψ between the direction of applied shear stress and the direction of particle motion decreases as the Shields stress τ_* increases. This feature is known to be relevant to, for example, the process of transverse sorting of grain size mixtures in meandering rivers [*Parker and Andrews*, 1985; *Seminara et al.*, 1997].

[55] The failure of the Bagnold constraint on an arbitrarily sloping bed is demonstrated in the next section.

6. Failure of the Bagnold Formulation on an Arbitrarily Sloping Bed

[56] Reducing (57) with the aid of (58) it is found that

$$\boldsymbol{\tau}_{fb} = \boldsymbol{\tau}_{fB} - \mu_d\rho(s-1)g\xi\left(|\boldsymbol{k}_n|\hat{s}_p - \frac{\boldsymbol{k}_t}{\mu_d}\right) \tag{69a}$$

Reducing the above equation with (60) yields the alternative form

$$\boldsymbol{\tau}_{fb} = \boldsymbol{\tau}_{fB} - \boldsymbol{\tau}_D \tag{69b}$$

where

$$\boldsymbol{\tau}_D = \frac{3c_D}{4D}\xi|\boldsymbol{U} - \boldsymbol{V}_P|(\boldsymbol{U} - \boldsymbol{V}_P) \tag{69c}$$

The straightforward generalization to the Bagnold constraint for the case of an arbitrarily sloping bed is the statement

$$|\boldsymbol{\tau}_{fb}| = \tau_{fc} \tag{70}$$

Imposing (70) on (69a) and expressing the result in dimensionless form using (2f), (48a), (60) and (61b) yields the following predictive relation for areal concentration $\hat{\xi}$;

$$\frac{\tau_{*c}}{\mu_d} = \left|\frac{\tau_*}{\mu_d}\hat{s} - \hat{\xi}\left(|\boldsymbol{k}_n|\hat{s}_p - \frac{\boldsymbol{k}_t}{\mu_d}\right)\right| \tag{71}$$

[57] It is immediately seen that in the case of one-dimensional flow over a horizontal bed ($\hat{s} \times \hat{s}_p = 0$, $|\boldsymbol{k}_n| = 1$, $\boldsymbol{k}_t = 0$) (71) reduces to the relation (34) for $\hat{\xi}$. Further evaluation of μ_d as 1.515 recovers the limiting case of (12) corresponding to the MFLvB form for areal bed load concentration for a horizontal bed.

[58] In point of fact, however, solutions for $\hat{\xi}$ to (71) fail to exist for transverse bed angles φ above some limiting value φ_{max} that is well below the angle of repose. As the stream-wise bed angle α increases above 0, the limiting
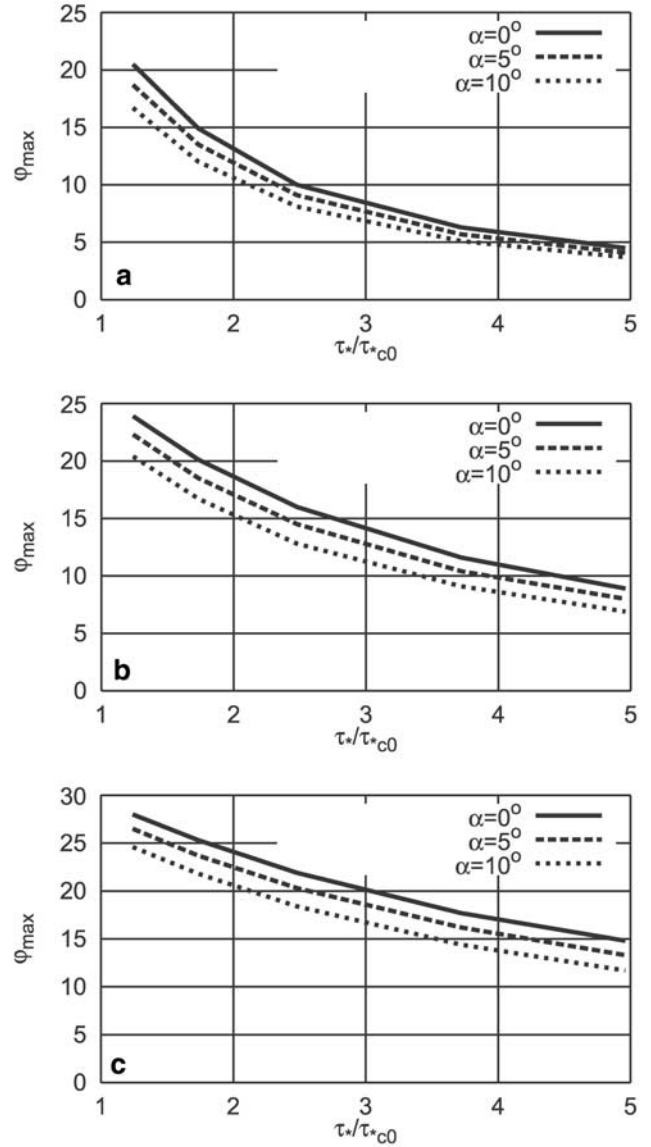

Figure 9. (a) Plot of maximum transverse angle φ_{max} as a function of τ_{*c}/τ_{*co} for three stream-wise angles, and with $\mu = 0.30$. (b) Plot of maximum transverse angle φ_{max} as a function of τ_{*c}/τ_{*co} for three stream-wise angles, and with $\mu = 0.70$. (c) Plot of maximum transverse angle φ_{max} as a function of τ_{*c}/τ_{*co} for three stream-wise angles, and with $\mu = 1.515$.

transverse angle φ_{max} above which solutions fail to exist further decreases. The demonstration of this failure is rather tedious, and is thus presented in Appendix A. The failure of the Bagnold criterion to predict an areal concentration $\hat{\xi}$ of equilibrium bed load transport on even relatively mild transverse slopes clearly demonstrates that the criterion cannot be correct, even in the case of a nearly horizontal bed.

[59] The results of the analysis given in Appendix A can be summarized as follows. In Figures 9a, 9b, and 9c, φ_{max} is plotted against τ_*/τ_{*co} for the angles $\alpha = 0°$, $5°$ and $10°$. The calculation was performed with the parameters $\lambda = 0.7$, $f = 11.5$, $\phi_r = \tan^{-1}(\mu) = 35°$, $\tau_{*c0} = 0.04$ and the three

values $\mu_d = 0.30$ (Figure 9a), 0.70 (Figure 9b) and 1.515 (Figure 9c). The unreasonable value of 1.515 obtained from a force-fitting of the Bagnold constraint to the data of *Fernandez Luque and van Beek* [1976] is used here only in full cognizance of the fact that *Bagnold* [1973] asserts that μ_d should not exceed, and indeed should be equal to μ, which is here assumed to take the value 0.70.

[60] As can be seen in Figures 9a, 9b, and 9c, φ_{max} decreases with increasing τ_*/τ_{*co} and α. For example, for the case $(\mu_d, \tau_*/\tau_{*co}) = (0.30, 4)$ and an angle $\alpha = 0°$, φ_{max} is only 6°; as α increases to 10° φ_{max} drops to 5° (Figure 9a). Even if μ_d is increased to the unrealistically high value of 1.515 at the same value of τ_*/τ_{*co}, φ_{max} is only 17° at $\alpha = 0$, dropping to 14° as α increases to 10° (Figure 9c). These values of φ_{max} are well below the angle of repose, confirming the failure of the Bagnold criterion.

[61] The analysis presented above is intended to be the simplest and most direct generalization of the Bagnoldean formulation traditionally given for the case of a nearly horizontal bed to the case of a bed with finite tilt in both the stream-wise and transverse directions. It is important to realize, however, that the failure illustrated above is not a consequence of the details of this generalization, but rather of the Bagnold formulation itself. That is, (70) is inconsistent with momentum balance for transverse slope angles above very modest maximum values that are well below the angle of repose.

[62] Although the reasons are not clearly discussed in the paper, the work of *Kovacs and Parker* [1994] represents an attempt to overcome the above failure of the Bagnold hypothesis in the simplest possible way. In particular, the constraint (70) is replaced with the constraint

$$\boldsymbol{\tau}_{fb} \cdot \boldsymbol{s} = \tau_{fc} \tag{72}$$

This implies that only the component fluid stress at the bed in the direction of the applied shear stress must drop to the critical value. Imposing this condition on (69) allows for the following solution for $\hat{\xi}$;

$$\hat{\xi} = \frac{1}{\left(|\boldsymbol{k}_n|\hat{\boldsymbol{s}}_p - \frac{\vec{k}_t}{\mu_d}\right) \cdot \hat{\boldsymbol{s}}} \frac{1}{\mu_d}\left(\tau_* - \tau_{*c}\right) \tag{73}$$

This relation reduces to (34) in the case of one-dimensional flow over a horizontal bed ($\hat{\boldsymbol{s}} \times \hat{\boldsymbol{s}}_p = 0$, $|\boldsymbol{k}_n| = 1$, $\boldsymbol{k}_t = 0$). In addition, (73) provides a well-behaved solution even under conditions for which (71) fails. This good behavior, however, is gained at the expense of an ad hoc assumption, (72), which has no obvious physical justification.

[63] Based on the above considerations, then, the Bagnold hypothesis should be completely abandoned in favor of an alternative entrainment hypothesis. This is the subject of G. Parker et al. (submitted manuscript, 2002).

[64] Several aspects of the analysis presented above leave room for refinement. For example, (42a), in which the effective layer-averaged stream-wise flow velocity U acting on the saltating bed load layer is related to the shear velocity u_τ that would prevail in the absence of bed load transport, can be replaced with a model in which the effect of the bed load transport on U is specifically computed. The layer-integrated bed load formulation presented here is not

sufficient to capture this feature. The model presented by *McEwan et al.* [1999] for the case of bed load transport on a nearly horizontal bed, however, does capture it, and again indicates a failure of the Bagnold hypothesis for the case studied therein.

7. Conclusion

[65] The above analysis indicates two deficiencies in regard to the Bagnold constraint. Firstly, it can explain the data of FLvB on nearly horizontal beds only at the expense of a coefficient of dynamic Coulomb friction that is well above the angle of repose. Secondly and more crucially, the Bagnold constraint yields no solution for areal bed load concentration, and thus the bed load transport rate itself for transverse bed slopes that are typically well below the angle of repose, and can be as low as a few degrees.

[66] The Bagnold hypothesis, according to which the mean fluid shear stress at the bed is reduced to the critical value for sediment motion, should thus be abandoned. The mechanistic framework presented here sets the stage for an alternative formulation presented by *Parker et al.* [submitted] that neither satisfies nor requires the Bagnold constraint.

Appendix A: Method of Calculation Demonstrating the Failure of the Bagnold Formulation

[67] The reason for the failure can be illustrated by reducing (54) with (59) to get

$$\boldsymbol{\tau}_{fb} = \boldsymbol{\tau}_{fB} - \frac{\xi}{\forall}\boldsymbol{F}_{Db} \tag{A1}$$

where

$$\forall = \frac{4}{3}\pi\left(\frac{D}{2}\right)^3 \tag{A2}$$

denotes the volume of a particle and

$$\boldsymbol{F}_{Db} = \frac{1}{2}\rho\pi\left(\frac{D}{2}\right)^2 c_D|\boldsymbol{U} - \boldsymbol{V}_P|(\boldsymbol{U} - \boldsymbol{V}_P) \tag{A3}$$

denotes the representative tangential drag force operating on the bed load layer. The Bagnold constraint (70) reduces (A1) to the form

$$\tau_{fc} = \sqrt{\tau_{fB}^2 + \left(\frac{\xi}{\forall}F_{Db}\right)^2 - 2\frac{\xi}{\forall}F_{Db}\tau_{fB}\cos\beta} \tag{A4}$$

where F_{Db} denotes the magnitude of $\boldsymbol{F}_{Db}$ and β denotes the angle between the vectors $\boldsymbol{\tau}_{fB}$ and $\boldsymbol{F}_{Db}$ ($|\beta| < \pi/2$). The left-hand side of (A4) possesses a minimum, however, when ξ takes the value

$$\xi_{lim} = \frac{\tau_{fB}\forall}{F_{Db}}\cos\beta \tag{A5a}$$

at which

$$\sqrt{\tau_{fB}^2 + \left(\frac{\xi_{lim}}{\forall}F_{Db}\right)^2 - 2\frac{\xi_{lim}}{\forall}F_{Db}\tau_{fB}\cos\beta} = \tau_{fB}\sin\beta \tag{A5b}$$
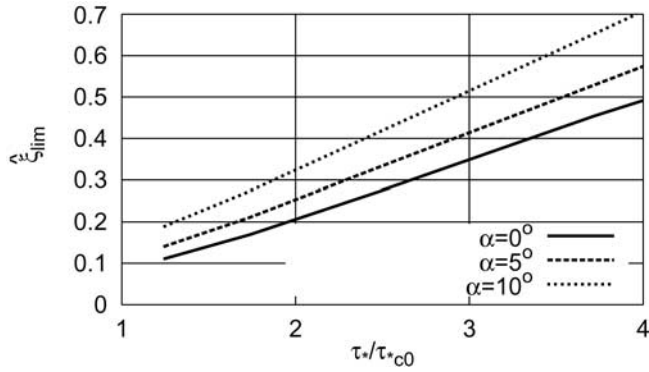
Figure 10. Plot of $\hat{\xi}_{lim}$ as a function of τ_{*c}/τ_{*co} for three transverse angles α and with $\mu = 0.30$.

If the right-hand side of (A5b) exceeds τ_{fc}, then, there is no way that (A4) can be satisfied. That is, the fluid shear stress at the bed cannot be reduced to the critical value no matter how large the areal concentration ξ is.

[68] Figure 10 shows a plot of the dimensionless form $\hat{\xi}_{lim}$ as a function of τ_*/τ_{*co} for three values of α, i.e. $\alpha = 0°$, $5°$ and $10°$. Note that the value of $\hat{\xi}_{lim}$ increases with increasing values of both τ_*/τ_{*co} and α. All other parameters are the same as that used in Figure 9a.

[69] The method used to extract the information from (71), (69a), and (69b) shown in Figures 9 and 10 is outlined below. The generalized Bagnold constraint can be expressed as follows;

$$\frac{|\boldsymbol{\tau}_{fb}|}{\rho(s - 1)gD} = \tau_{*c}(\alpha', \varphi') \qquad (A6)$$

where τ_{*c} is the critical Shields stress associated with the longitudinal slope α' and the transverse slope φ'. Here (α', φ') denote the values (α, φ) of associated with the residual stress vector $\boldsymbol{\tau}_{fb}$ in (69). Evaluating (69) in terms of these angles requires some tedious, though straightforward algebraic manipulation.

[70] The unit vector of the horizontal axis obtained by projecting the residual shear stress vector $\boldsymbol{\tau}_{fb}$ onto the horizontal plane passing through point P is denoted as $\hat{\mathbf{x}}_b$. In addition, the unit vector of the horizontal axis orthogonal to $\hat{\mathbf{x}}_b$ is denoted as $\hat{\mathbf{x}}'_p$. It is then possible to write

$$\tan \alpha' = -\nabla \eta \cdot \hat{\mathbf{x}}_b \qquad (A7a)$$

$$\tan \varphi' = -\nabla \eta \cdot \hat{\mathbf{x}}'_p \qquad (A7b)$$

Furthermore, if the unit vector $\boldsymbol{\tau}_{fb}/|\boldsymbol{\tau}_{fb}|$ is denoted as $\hat{\mathbf{s}}_b$, then

$$\hat{\mathbf{x}}_b = \frac{(\hat{\mathbf{k}} \times \hat{\mathbf{s}}_b) \times \hat{\mathbf{k}}}{|(\hat{\mathbf{k}} \times \hat{\mathbf{s}}_b) \times \hat{\mathbf{k}}|} \qquad (A8a)$$

$$\hat{\mathbf{x}}'_p = \frac{\hat{\mathbf{k}} \times \hat{\mathbf{s}}_b}{|\hat{\mathbf{k}} \times \hat{\mathbf{s}}_b|} \qquad (A8b)$$

or reducing with (69c),

$$\hat{\mathbf{x}}_b = \frac{(\hat{\mathbf{k}} \times \boldsymbol{\tau}_{fB}) \times \hat{\mathbf{k}} - (\hat{\mathbf{k}} \times \boldsymbol{\tau}_D) \times \hat{\mathbf{k}}}{|(\hat{\mathbf{k}} \times \boldsymbol{\tau}_{fB}) \times \hat{\mathbf{k}} - (\hat{\mathbf{k}} \times \boldsymbol{\tau}_D) \times \hat{\mathbf{k}}|} \qquad (A9a)$$

$$\hat{\mathbf{x}}'_p = \frac{(\hat{\mathbf{k}} \times \boldsymbol{\tau}_{fB}) - (\hat{\mathbf{k}} \times \boldsymbol{\tau}_D)}{|(\hat{\mathbf{k}} \times \boldsymbol{\tau}_{fB}) - (\hat{\mathbf{k}} \times \boldsymbol{\tau}_D)|} \qquad (A9b)$$

[71] A considerable amount of algebra performed on (A9a) and (A9b) using the definitions (39), (40), (46), (47) and (66) eventually leads to the following relationships;

$$\hat{\mathbf{x}}_b = \hat{\mathbf{x}}_\tau \frac{1 - PM}{Q} + \frac{PR}{Q}\left(-\sin \alpha \tan \varphi, \frac{1}{\cos \alpha}, 0\right) \qquad (A10)$$

$$\hat{\mathbf{x}}'_p = \frac{1}{N'}\left\{-\frac{PR}{\cos \alpha}, [\cos \alpha(1 - PM) - PR \sin \alpha \tan \varphi], 0\right\} \qquad (A11)$$

where

$$M = f\sqrt{\tau_*} - \hat{V}_P \cos \psi \qquad (A12a)$$

$$P = \frac{3}{4}c_D\hat{\xi}\frac{\sqrt{M^2 + \hat{V}_P^2 \sin^2 \psi}}{\tau_*} \qquad (A12b)$$

$$R = \frac{\hat{V}_P \sin \psi}{\sqrt{1 + \tan^2 \alpha + \tan^2 \varphi}} \qquad (A13)$$

$$Q = \left\{[1 - P(M + R \sin \alpha \tan \varphi)]^2 + \left[\frac{PR}{\cos \alpha}\right]^2\right\}^{1/2} \qquad (A14)$$

$$N = \left\{[\cos \alpha - P(M \cos \alpha + R \sin \alpha \tan \varphi)]^2 \right. $$
$$\left. + [-\sin \alpha - P(-M \sin \alpha + R \cos \alpha \tan \varphi)]^2 + \left[\frac{PR}{\cos \alpha}\right]^2\right\}^{1/2} \qquad (A15)$$

and

$$N' = \left\{\left[\frac{PR}{\cos \alpha}\right]^2 + [\cos \alpha - P(M \cos \alpha + R \sin \alpha \tan \varphi)]^2\right\}^{1/2} \qquad (A16)$$

Finally, with the use of (A10) and (A11) the definitions (A7), (A8) and (A9a) yield

$$\tan \alpha' = \frac{1}{Q}[(1 - PM) \sin \alpha + PR \tan \varphi \cos \alpha] \qquad (A17a)$$

$$\tan \varphi' = \frac{1}{Q}\left[(1 - PM) \tan \varphi \cos \alpha - PR \sin \alpha\left(\frac{1}{\cos^2 \alpha} + \tan^2 \varphi\right)\right] \qquad (A17b)$$

The above relationships allow the evaluation of the angles α' and φ' as functions of, $\hat{\xi}$, α, φ, τ_* and ψ.

[72] The above relations can be used to reinforce the exact generalization of the Bagnold constraint. Equations (61b) and (47) are used to rephrase the quantity $\tau_{fB}/|\tau_{fB}|$. In addition, the definitions (61a) and (61d) for U and (65) for V_P can be used to rephrase the relation (69c) for τ_D. With some further manipulation (69b) can be reduced to the form

$$\left|\boldsymbol{\tau}_{fb}\right| = \left|\boldsymbol{\tau}_{fB} - \boldsymbol{\tau}_D\right| = N\left|\boldsymbol{\tau}_{fB}\right| \qquad (A18)$$

From (A18), then, the generalized Bagnold constraint takes the form

$$\tau_* = \frac{\tau_{*c}\left[\alpha'\left(\hat{\xi}\right), \varphi'\left(\hat{\xi}\right)\right]}{N\left(\hat{\xi}\right)} \qquad (A19)$$

The problem thus reduces to an implicit equation for the unknown areal concentration $\hat{\xi}$ which can be solved iteratively. It is this procedure which has been used to generate Figures 9 and 10. This same procedure yields for any given value of τ_*/τ_{*c} a threshold value of transverse slope φ above which no solution for $\hat{\xi}$ can be found.

Notation

A, A' parameters defined by (68a) and (68b), respectively
B dimensionless parameter in (43a) which takes the value 30 for fully rough turbulent flow
c local mean volume concentration of particles participating in bed load transport
C layer-averaged mean volume concentration of particles participating in bed load transport
c_D particle drag coefficient
c_L particle lift coefficient
D grain size
D_b volume rate of particle deposition per unit bed area
$\hat{D}$ dimensionless version of D_b defined by (2e)
E_b volume rate of particle erosion (pickup) per unit bed area
$\hat{E}$ dimensionless version of E_b defined by (2d)
$\hat{E}_a$ rescaled version of $\hat{E}$ defined by (5d)
f $= U/u_\tau$ in accordance with (29); $= 11.5$ based on (4c)
F_b bed surface defined in equation (36)
F_D magnitude of drag force on a particle
$\boldsymbol{F}_D$ vectorial generalization of F_D
$\boldsymbol{F}_{Db}$ effective drag acting on a bed load particle defined by (A3)
F_L magnitude of lift force on a particle
$\boldsymbol{F}_D$ vectorial generalization of F_L
g acceleration of gravity
G_s magnitude of the submerged weight of a particle, defined by (41f)
$\boldsymbol{G}_s$ vectorial generalization of G_s
H flow depth
h_s mean height of the bed load layer
$\hat{k}$ upward vertical unit vector
$\boldsymbol{k}_n$ normal component of $(-\hat{k})$
k_s roughness height of the bed
$\boldsymbol{k}_t$ transverse component of $(-\hat{k})$
L_s mean saltation length

$\hat{L}_s$ dimensionless version of L_s defined by (2g)
L_{step} mean step length
$\hat{L}_{step}$ dimensionless version of L_{step} defined by (2h)
M parameter defined by (A12a)
N parameter defined by (A15)
N' parameter defined by (A16)
$\hat{\boldsymbol{n}}$ unit vector upward normal to the bed
n_k dimensionless parameter relating roughness height k_s to grain size D defined in (43b)
P parameter defined by (A12b)
p_{ls} local mean pressure (or the negative of the normal stress) of the solid phase at elevation z above the bed
p_{sb} value of p_{lb} at the bed
Q parameter defined by (A14)
q volume sediment transport rate per unit width
$\hat{q}$ dimensionless Einstein bed load transport rate defined by (2a)
$\hat{\boldsymbol{q}}$ vectorial generalization of $\hat{q}$
$\hat{q}_a$ rescaled version of $\hat{q}$ defined by (5a)
R parameter defined by (A13)
r_L parameter describing the effect of lift defined in (51b)
S magnitude of bed slope
s specific gravity of sediment
$\hat{\boldsymbol{s}}$ unit vector in the direction of $\boldsymbol{\tau}_{fB}$
$\hat{\boldsymbol{s}}_b$ unit vector in the direction of $\boldsymbol{\tau}_{fb}$
$\hat{\boldsymbol{s}}_p$ unit vector in the direction of V_P
T_{fsx} value of t_{fsx} resulting from averaging over the bed load layer
$\boldsymbol{t}_{fs}$ vectorial rate of transfer of momentum per unit volume per unit time from the fluid phase to the solid phase
t_{fsx} stream-wise component of $\boldsymbol{t}_{fs}$
t_{fsz} upward normal component of $\boldsymbol{t}_{fs}$
U stream-wise component of $\boldsymbol{u}$ averaged over the bed load layer
$\boldsymbol{u}$ local vectorial mean velocity of the fluid phase at elevation z in the bed load layer
u_τ shear velocity defined by (28)
$u_{\tau c}$ critical shear velocity
V_P layer-averaged mean velocity of bed load particles
$\hat{V}_P$ dimensionless version of V_P defined by (2c)
$\boldsymbol{v}$ local vectorial mean velocity of the solid phase at elevation z in the bed load layer
$\hat{\boldsymbol{x}}_b$ unit vector defined by (A8a)
x_p horizontal axis lying orthogonal to the vertical plane $(\tau_{fB}, \hat{k})$
$\hat{\boldsymbol{x}}_p$ unit vector in the direction of x_p
$\hat{x}'_p$ unit vector defined by (81b)
x_τ horizontal axis lying in the vertical plane $(x_\tau, \hat{k})$
$\hat{\boldsymbol{x}}_\tau$ unit vector in the direction of x_τ
z vertical distance upward from the bed
α stream-wise bed angle
α' stream-wise angle of the vector τ_{fb}
β angle between the vectors τ_{fB} and $\boldsymbol{F}_{Db}$
χ $= \tau_*/\tau_{*c}$ or τ_*/τ_{*co}
Δ parameter describing the effect of lift defined by (51a)
ϕ_r angle of repose, $= \tan^{-1}(\mu)$
η bed elevation
φ transverse bed angle
φ' transverse angle of the vector τ_{fb}

κ Karman constant of 0.40

λ dimensionless coefficient relating the Shields stress necessary for bed load transport to stop to the critical Shields stress for the initiation of bed load transport

λ_o value of λ on a nearly horizontal bed; $= 0.7$ based on (4c).

μ coefficient of static friction

μ_d coefficient of dynamic friction

μ_{do} coefficient of dynamic friction on a nearly horizontal bed

ν kinematic viscosity of water

ρ density of water

$\boldsymbol{\tau}_D$ effective "drag stress" defined by (69c)

τ_{fB} mean fluid bed shear stress that would prevail in the absence of bed load transport

$\boldsymbol{\tau}_{fB}$ vectorial generalization of τ_{fB}

τ_{fb} magnitude of mean fluid shear stress at the bed in the presence of a bed load layer

τ_{fco} critical fluid shear stress at the bed for the initiation of bed load

τ_{fI} magnitude of mean fluid shear stress at the interface between the bed load layer and the fluid above

τ_{lf} local mean stream-wise fluid shear stress at distance z above the bed

τ_{ls} local mean stream-wise shear stress of the solid phase at distance z above the bed

τ_{sb} magnitude of mean shear stress exerted on the bed by the solid phase (particle collision)

$\boldsymbol{\tau}_{sb}$ vectorial generalization of τ_{sb}

τ_* Shields stress based on τ_{fB}

$\boldsymbol{\tau}_*$ vectorial generalization of τ_*

τ_{*c} critical Shields stress on an arbitrarily sloping bed

τ_{*co} critical Shields stress on a nearly horizontal bed

τ_{*cso} critical Shields stress for the cessation of bed load motion, defined by (30)

τ_* dimensionless form of τ_{fB} defined by (2b)

ω vorticity of the flow acting on a "dangerously placed" bed particle

ξ volume areal concentration of bed load such that $\xi = Ch_s$

$\hat{\xi}$ dimensionless version of ξ defined by (2f)

ψ angle between the direction of the applied shear stress and the direction of particle velocity

ζ elevation above the bed used for the evaluation of the lift force

$\forall$ particle volume defined by (A2)

References

Abbott, J. E., and J. R. D. Francis, Saltation and suspension trajectories of solid grains in a water stream, *Philos. Trans. R. Soc. London, Ser. A, 284,* 225–254, 1977.

Ashida, K., and M. Michiue, Study on hydraulic resistance and bedload transport rate in alluvial streams, *Trans. Jpn. Soc. Civil Eng., 206,* 59–69, 1972.

Auton, T. R., The lift force on a spherical body in a rotational flow, *J. Fluid Mech., 183,* 199–218, 1987.

Auton, T. R., J. C. R. Hunt, and M. Prud'homme, The force exerted on a body in inviscid unsteady non-uniform rotational flow, *J. Fluid Mech., 197,* 241–257, 1988.

Bagnold, R. A., The flow of cohesionless grains in fluids, *Philos Trans. R. Soc. London, Ser. A, 249,* 235–297, 1956.

Bagnold, R. A., The nature of saltation and "bed-load" transport in water, *Proc. R. Soc. London, Ser. A, 332,* 473–504, 1973.

Bridge, J. S., and S. J. Bennett, A model for the entrainment and transport of sediment grains of mixed sizes, shapes and densities, *Water Resour. Res., 28*(2), 337–363, 1992.

Chepil, W. S., The use of evenly spaced hemispheres to evaluate aerodynamic forces on a soil surface, *Eos Trans. AGU, 39*(3), 397–404, 1958.

Engelund, F., and J. Fredsoe, A sediment transport model for straight alluvial channels, *Nord. Hydrol., 7,* 293–306, 1976.

Fernandez Luque, R., and R. van Beek, Erosion and transport of bedload sediment, *J. Hydraul. Res., 14*(2), 127–144, 1976.

Einstein, H. A., The bedload function for sediment transportation in open channel flow, *Tech. Bull. U.S. Dep. Agric., 1026,* 1950.

Graf, W., *Hydraulics of Sediment Transport*, 513 pp., McGraw-Hill, New York, 1971.

Ikeda, S., Incipient motion of sand particles on side slopes, *J. Hydraul. Eng., 108*(1), 95–114, 1982.

Kovacs, A., and G. Parker, A new vectorial bedload formulation and its application to the time evolution of straight river channels, *J. Fluid Mech., 267,* 153–183, 1994.

McEwan, I. K., B. J. Jefcoate, and B. B. Willetts, The grain-fluid interaction as a self-stabilizing mechanism in fluvial bedload transport, *Sedimentology, 46,* 407–416, 1999.

Nakagawa, H., and T. Tsujimoto, Sand bed instability due to bed-load motion, *J. Hydraul. Eng., 106*(12), 2029–2051, 1980.

Nino, Y., and M. Garcia, Gravel saltation, 1, Experiments, *Water Resour. Res., 30*(6), 1907–1914, 1994a.

Nino, Y., and M. Garcia, Gravel saltation, 2, Modeling, *Water Resour. Res., 30*(6), 1915–1924, 1994b.

Nino, Y., and M. Garcia, Using Lagrangian particle saltation observations for bedload sediment transport modeling, *Hydrol. Processes, 12*(8), 1197–1218, 1999.

Owen, P. R., Saltation of uniform grains in air, *J. Fluid Mech., 20*(2), 225–242, 1964.

Parker, G., and E. D. Andrews, Sorting of bed load sediment by flow in meander bends, *Water Resour. Res., 21*(9), 1361–1373, 1985.

Schmeeckle, M. W., A dynamic boundary condition for bedload sediment transport in non-uniform, hydraulically rough turbulent boundary layers, *Annu. J. Hydraul. Eng. Jpn. Soc. Civ. Eng., 43,* 653–658, 1999.

Sekine, M., and H. Kikkawa, Mechanics of saltating grains, *J. Hydraul. Eng., 118*(4), 536–558, 1992.

Sekine, M., and G. Parker, Bedload transport on transverse slopes, *J. Hydraul. Eng., 118*(4), 513–535, 1992.

Seminara, G., L. Solari, and M. Tubino, Finite amplitude scour and grain sorting in wide channel bends, paper presented at 27th IAHR Congress, Int. Assoc. for Hydraul. Res., San Francisco, Calif., 10–15 Aug. 1997.

Tsujimoto, T., Mechanics of sediment transport of graded materials and fluvial sorting, report (in Japanese and English), Fac. of Eng., Kanazawa Univ., Kanazawa, Japan, 1991.

van Rijn, L., Sediment pick-up functions, *J. Hydraul. Eng., 110*(10), 1494–1502, 1984.

Wiberg, P. L., and J. D. Smith, A theoretical model for saltating grains in water, *J. Geophys. Res., 90*(C4), 7341–7354, 1985.

Wiberg, P. L., and J. D. Smith, Model for calculating bedload transport of sediment, *J. Hydraul. Eng, 115*(1), 101–123, 1989.

———————————

G. Parker, St. Anthony Falls Laboratory, University of Minnesota, Minneapolis, MN, 55414, USA. (parke002@tc.umn.edu)

G. Seminara, Dipartimento di Ingegneria Ambientale, Universita degli Studi di Genova, Via Montallegro 1, 16145, Genova, Italy. (sem@diam. unige.it)

L. Solari, Dipartimento di Ingegneria Civile, Universita degli Studi di Firenze, Via S. Marta 3, 50139, Firenze, Italy. (luca.solari@dicea.unifi.it)